High capacitance of coarse-grained carbide derived carbon electrodes

Boris Dyatkin [a], Oleksiy Gogotsi [b], Bohdan Malinovskiy [b], Yuliya Zozulya [b], Patrice Simon [c], Yury Gogotsi [a,*]

[a] Department of Materials Science & Engineering, and A.J. Drexel Nanomaterials Institute, Drexel University, Philadelphia, PA 19104, USA
[b] Materials Research Centre, 03680 Kyiv, Ukraine
[c] Université Paul Sabatier-Toulouse III, Laboratoire CIRIMAT, UMR 5085, 31062 Toulouse Cedex 4, France

HIGHLIGHTS

- High capacitance and power density of coarse-grained porous carbon supercapacitors.
- Lower synthesis and manufacturing costs.
- Greater mass loading for grid and automotive electrical energy storage.
- Superior performance than activated carbon in different electrolytes.
- Expanded operating voltage window.

GRAPHICAL ABSTRACT

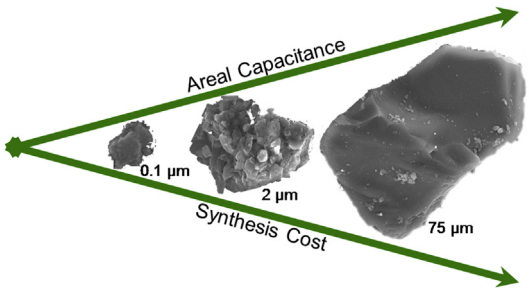

ABSTRACT

We report exceptional electrochemical properties of supercapacitor electrodes composed of large, granular carbide-derived carbon (CDC) particles. Using a titanium carbide (TiC) precursor, we synthesized 70–250 μm sized particles with high surface area and a narrow pore size distribution. Electrochemical cycling of these coarse-grained powders defied conventional wisdom that a small particle size is strictly required for supercapacitor electrodes and allowed high charge storage densities, rapid transport, and good rate handling ability. The material showcased capacitance above 100 F g^{-1} at sweep rates as high as 250 mV s^{-1} in organic electrolyte. 250–1000 micron thick dense CDC films with up to 80 mg cm^{-2} loading showed superior areal capacitances. The material significantly outperformed its activated carbon counterpart in organic electrolytes and ionic liquids. Furthermore, large internal/external surface ratio of coarse-grained carbons allowed the resulting electrodes to maintain high electrochemical stability up to 3.1 V in ionic liquid electrolyte. In addition to presenting novel insights into the electrosorption process, these coarse-grained carbons offer a pathway to low-cost, high-performance implementation of supercapacitors in automotive and grid-storage applications.

Keywords:
Supercapacitor
Carbide-derived carbon
Electrode material
Energy density
Grid storage
Porous carbon

1. Introduction

Electrochemical capacitors (also known as supercapacitors or ultracapacitors), which rely on the electrosorption of ions by porous carbon electrodes, offer high power densities [1,2]. They are attracting increasing interest and are showing growing promise in automotive, personal electronics, and grid-scale electrical energy storage systems [3]. The charge storage mechanism of supercapacitors facilitates rapid charge transport and is more efficient than transport-limited redox and intercalation processes of

* Corresponding author.
E-mail address: gogotsi@drexel.edu (Y. Gogotsi).

traditional batteries. Subsequently, they offer up to 15 kW kg^{-1} power densities and a very large operating cycle life. However, the electrosorption process is not energy-dense and can offer only 6 Wh kg^{-1} [4]. Many applications, such as wearable electronics or hand-held devices, require supercapacitors with high volumetric capacitance and large areal electrode mass loading [5,6]. Since energy density is exponentially dependent on applied potential, the next generation of supercapacitors must rely on electrode and electrolyte combinations that exceed the current ~2.7 V window limit [7]. Finally, the material costs of electrochemical capacitors must remain low for them to become viably competitive with batteries, fuel cells, and other energy storage systems.

Existing commercial supercapacitors predominantly implement activated carbon with the particle size of a few microns. It is commonly derived from biomass (coconut shells, wood char, or peat bog) using chemical or physical activation at 800–900 °C [8]. Carbide derived carbons (CDCs), which are synthesized *via* Cl_2 (g) etching of metal carbides (TiC, SiC, Mo_2C, B_4C, etc.) at 200–1200 °C, offer high specific surface areas (1000–2000 m^2 g^{-1}) and tunable [9], monodisperse porosities [10,11]. Since their pore diameter (5 Å < d_{pore} < 11 Å) can be selected to match the size of electrosorbed ions, CDCs have demonstrated exceptional capacitance of over 150 F g^{-1} in non-aqueous electrolytes [12,13]. Furthermore, their thermal and electrochemical stability makes them a promising supercapacitor carbon alternative [10]. Stemming from high porosity of these materials, the Cl_2 + metal carbide reaction proceeds at a linear rate (for grains <80 μm thick) with minimal transport limitations [14]. From CDCs that had been analyzed in electrochemical capacitors, those derived from TiC precursors (TiC-CDCs) have subnanometer pores and offer the highest charge storage densities [15]. However, similar to other well-tuned internal pore structures (such as templated mesoporous carbons and activated graphene), CDC synthesis process has not been sufficiently cost-effective for these materials to become economically competitive with activated carbon. At the same time, they offer an excellent model system for studying fundamental aspects of charge storage in porous carbons.

A viable approach that improves the scalability of CDC synthesis minimizes the cost of carbide precursors. Since carbides undergo a conformal transformation during synthesis [16], their starting dimensions are identical to those of desired CDC particles (1–5 μm diameters). Prolonged milling and sieving, which is required to produce micron-sized TiC powders, makes them significantly more expensive than coarse, abrasive carbide powders. Other previously reported supercapacitors, which were composed of nanosized CDC electrode particles [17], had relied on high-energy plasma synthesis of 20 nm TiC precursor nanopowders [18]. If future supercapacitor electrodes can successfully implement coarse-grained, large carbon (CDC or activated carbon) electrodes, these devices will become much more economically viable. However, all commercial devices use small carbon particles and a previous study on SiC-CDC [19] showed that capacitance increases with decreasing particle size in the range from 30 nm to 20 μm. No attention has been paid to larger particles, as it has been known that long pore lengths may impede ion mobility [19–23]. However, recent *in situ* FTIR spectroelectrochemistry experiments have shown that electrosorption predominantly involves short-range interactions (<10 nm), and bulk transport of electrolyte across the cell is not a rate-limiting step [24]. Furthermore, we have demonstrated rectangular cyclic voltammograms (CV) high charge storage densities and good rate handling abilities in flow supercapacitor cells, which rely on a slurry suspension of granular (100–200 μm) microporous activated carbon beads [25,26]. The latter work underscores the importance of a good electron transport network through the electrode, and shows that large particles may deliver high capacitance. However, those powders were suspended in electrolyte – a different arrangement compared to polymer-bonded electrode films. Monolithic TiC-CDC films showed excellent capacitance [27,28], but this result could not be scaled to thicker CDC plates (250 μm thicknesses) [29,30].

Our objective is to study capacitance and rate handling capabilities of coarse-grained porous carbon powders in supercapacitors. Our approach relies on commercial-grade abrasive TiC powder, which is significantly less expensive than microscale or nanoscale powders, with minimal synthesis and processing steps. We demonstrate superior performance of resulting electrode films in different electrolytes compared to conventional activated carbons. From a fundamental perspective, this finding highlights the significance of short-range interactions and stresses the importance of development of novel charge electrosorption models. We demonstrate that ion behavior in narrow, confined pores is significantly different than that of double layer adsorption on flat, external surfaces [31,32]. In addition to greater capacitance, electrochemical stability of ions may improve due to minimized external surface and maximized confinement in narrow pores. Finally, porous particles with long and interconnected pores provide us with a novel model system to evaluate the influence of pore wall chemistry on capacitance and ion mobility. From a practical perspective, we introduce high-performing carbon electrodes with superior mass loading, gravimetric and volumetric energy densities, and reduced cost.

2. Experimental methods

2.1. Materials synthesis

The starting precursor material for all experiments was TiC powder (Reaktiv, Donetsk, Ukraine) with a 140–250 μm particle size. A ball mill ground up the material for 15 h (HDPE enclosure, TiC grinding media). A Ro-Tap particle sieving instrument separated the fraction containing 40–80 μm particles. TiC was converted to TiC-CDC according to a previously described procedure [33,34]. Particles were pelletized with polyvinyl acetate (PVA), loaded into a quartz boat, and placed into a horizontal tube furnace. A boat filled with activated carbon was placed in front of the TiC-containing one to remove oxygen or other impurities in the gas stream. The material was heated to 800 °C under a flowing Ar atmosphere (198 cm^3 min^{-1}). Subsequently, it was treated with Cl_2 (g) (370 cm^3 min^{-1}) at 800 °C for 6.5 h and H_2 (g) (492 cm^3 min^{-1}) at 600 °C for 2 h. The material was cooled under flowing Ar, removed, and weighted. Photographs of the boat before and after synthesis are shown in Fig. S1 in Supplementary Information (SI). This coarse powder material was used for the majority of the testing and is also referred to as "Initial CDC." Additionally, some 250 μm diameter TiC particles were converted to CDC using the same procedure without any milling. They are referred to as "Large CDC." For comparison of basic material properties and electrochemical performance, we used YP50 activated carbon (Kuraray, Okayama, Japan) and TiC-CDC and SiC-CDC micro- and nanopowders that were synthesized using the same method as described above.

Approximately 500 mg of initial CDC material was manually ground up in an agate mortar and pestle for 2 h. Water and ethanol were intermittently used to facilitate the pulverization process. The smaller-particle variant of the CDC powder is hereafter referred to as "Milled CDC."

2.2. Materials characterization

A Quadrasorb gas sorption analyzer (Quantachrome

Instruments, Boynton Beach, USA) measured the specific surface area (SSA) and pore size distribution (PSD) of CDCs. N_2 (g) sorption isotherms were collected at −196 °C using liquid N_2 coolant. Brunauer–Emmett–Teller (BET) SSA was calculated from 0.05 to 0.30 P/P_0 value range [35]. Pore volume and pore size distribution calculations were performed using Quenched Solid Density Functional Theory (QSDFT) analysis available from the Quadrawin (Quantachrome) instrument package [36]. We collected images and measured elemental composition using a Zeiss Supra 50VP Scanning Electron Microscope (SEM) with built-in Oxford Energy-Dispersive X-ray Microanalysis.

Thermogravimetric analysis (TGA) was performed using a Q50 Thermal Analyzer (TA Instruments, New Castle, USA) by placing the CDC powder sample in an alumina crucible and heating it in a flowing air atmosphere (10 ml min^{-1}) from 25 °C to 850 °C at a 5 °C min^{-1} ramping rate. TGA was also conducted in a flowing Ar atmosphere to calculate the functional group content on the surface of CDC powders [37]. To conduct X-ray diffraction (XRD) measurements, we used an Empyrean Series 2 Diffractometer (PANalytical, Netherlands) and conducted reflection mode measurements using a flat stage in the 5–90° 2θ range (0.026° step size, 3.03° min^{-1} rate). Raman spectroscopy measurements were made using a Renishaw inVia Spectrometer (Renishaw Instruments, Glouchestershire, UK) and a 633 nm He–Ne laser.

X-ray pair distribution function (PDF) analysis was performed at the 11-1D-B beamline of the Advanced Photon Source (Argonne National Laboratory). Synchrotron X-ray total scattering measurements analyzed powders in transmission mode. Scattering measurements used 58.65 keV incident radiation (0.2114 Å wavelength) in the 0.01 $Å^{-1}$ < Q < 22.2 $Å^{-1}$ range. The Fit2D program was used to calibrate the measurement and PDFGetX2 to derive S(Q) and G(r) plots. Extended Q range small-angle neutron scattering (EQ-SANS) measurements were completed at the BL-6B beamline of the Spallation Neutron Source (Oak Ridge National Laboratory). Measurements combined a 1.3 m sample to detector (SDD) distance (1.13–4.65 Å) and a 4.0 m SDD (2.61–5.61 Å and 9.51–12.91 Å) to obtain a broad Q range [38].

2.3. Electrochemical testing

Supercapacitor measurements used 90 μm, 250 μm, and 1000 μm (1 mm) thick electrode films prepared by mixing CDC powders with PTFE binder in a 95%–5% carbon-to-binder mass ratio, mixing the slurry in ethanol, and rolling the films using a manual rolling mill. A photograph of the film is shown in SI (Fig. S1). We punched circular disks (6.3 mm or 12 mm in diameter) and assembled them into 2-electrode pouch cells [39]. Supercapacitor cells used three different electrolytes: 1) a 1.5 M solution of tetraethylammonium tetrafluoroborate ($[NEt_4^+][BF_4^-]$, 99.9%, Fluka) in acetonitrile (CH_3CN, HPLC grade, Fisher Scientific), 2) a 50 wt.% dispersion of 1-ethyl-3-methylimidazolium bis(trifluoromethylsulfonyl)imide ($[EMim^+][TFSI^-]$, IoLiTec Ionic Liquids Technologies Inc.) in acetonitrile, and 3) neat $[EMim^+][TFSI^-]$. Films composed of 250 μm diameter CDC particles incorporated 5 wt.% carbon nanotubes (Arkema, 200 m^2 g^{-1}) as a conductive additive. We used L-shaped carbon-coated aluminum current collectors (Exopack) for the $[NEt_4^+][BF_4^-]$ experiments and Pt foil disks with L-shaped stainless steel backbones for the $[EMim^+][TFSI^-]$ experiments. 2 layers of Celgard sheets between the symmetrical electrodes acted as separators. All experiments were conducted in an Ar-filled glovebox. A Physical Property Measurement System (Quantum Design, San Diego) with an external current source (Keithley 6220, Ohio) and a nanovoltmeter (Keithley 2182A) measured sheet resistivity of electrode films. We attached gold wires to the films using silver paint and used a 4-point probe method to calculate electronic conductivity [40].

A VMP3 potentiostat (Bio-Logic, Grenoble, France) was used to conduct electrochemical measurements. Cyclic voltammetry (CV) sweeps in the 1 mV s^{-1} – 2000 mV s^{-1} range, galvanostatic cycling (GC) in the 0.1–5.0 A g^{-1} range, electrochemical impedance spectroscopy (EIS) in the 200 kHz–10 mHz range, and square wave amperommetry measurements provided gravimetric capacitance (C_{sp}), ionic and electronic resistance, rate handling ability, and electrochemical stability information. The Nyquist plot provided Equivalent Series Resistance (ESR) from the measurement of real impedance at its x-axis crossover. We calculated the ionic impedance of the electrodes, which is characteristic of ion transport resistance, by measuring the difference between the end of the high frequency loop characteristic of the contact impedance between the film and the current collector and the "knee" region of the Nyquist plot [41]. We calculated capacitance from discharge data and normalized the values to the single electrode mass.

3. Results and discussion

3.1. Materials synthesis and structure

Following synthesis, the remaining carbon powder mass (Fig. 1a) amounted to 12.8% of the starting TiC mass (compared to the 20% predicted from stoichiometry). Therefore, we expect that the material fully converted to a porous carbon with no Cl_2 or $TiCl_4$ transport limitations. Furthermore, TGA analysis (Fig. S2a in SI) of the carbon material revealed almost complete burn-off, with an ash content <2% (Table 1). XRD analysis (Fig. S3b in SI) did not demonstrate any distinctive TiC or TiO_2 peaks in the synthesized CDC material. Elemental analysis (Table S1 in SI) confirmed that only trace amounts of Ti and Cl remained in the material and that, subsequently, the synthesis method is suitable for synthesis of such large, coarse-grained carbon powders.

Porosity analysis (Fig. 1c) demonstrated a microporous structure of the material with a narrow pore size distribution. The SSA of the initial CDC (1822 m^2 g^{-1}) and its predominant pore diameter (0.67 nm) are very similar to the measurements that had been previously reported for ~1.0 μm-sized TiC-CDCs synthesized at 800 °C [33]. The isotherms are shown in Fig. S4 in SI. The synthesized powders resemble the irregularly shaped particles that are typical for CDCs produced from ball-milled carbide precursors. The overall particle shape does not change after mechanical milling (Fig. S1a in SI), and neither the SSA nor the porosity are affected by the grinding process. This suggests that, instead of collapsing pores, the procedure likely broke the particles in a brittle manner. The larger, 250 μm TiC-CDC particles exhibited equally high SSA and a narrow pore size distribution.

SANS data (Fig. S3a in SI) showed similar Q vs. I(Q) trends in the "flat" Guinier region (0.15 $Å^{-1}$ < Q < 0.5 $Å^{-1}$) for CDCs synthesized at 800 °C from differently sized carbide precursors, reinforcing the similarities in pore size distributions and their predominant dependence on Cl_2 treatment temperature [42,43]. However, the Q vs. I(Q) slopes diverged in the Porod region (0.01 $Å^{-1}$ < Q < 0.03 $Å^{-1}$), which suggests differences in scattering from surface and mass fractals and, subsequently, differences in pore surface corrugation (roughness). Raman spectra (Fig. S3c in SI) showed narrow D and G bands. Based on PDF analysis of *r* vs. *G*(*r*), the carbon is composed of a mixture of 5–, 6–, and 7–atom rings (Fig. S4 in SI) [44].

Based on the analysis of the structure and surface chemistry, we can conclude that synthesis of coarse-grained 75–250 μm diameter CDCs can effectively use the same Cl_2 furnace synthesis procedure that had been successfully implemented for micropowder and nanopowder CDCs. Large TiC particles fully converted to TiC-CDC

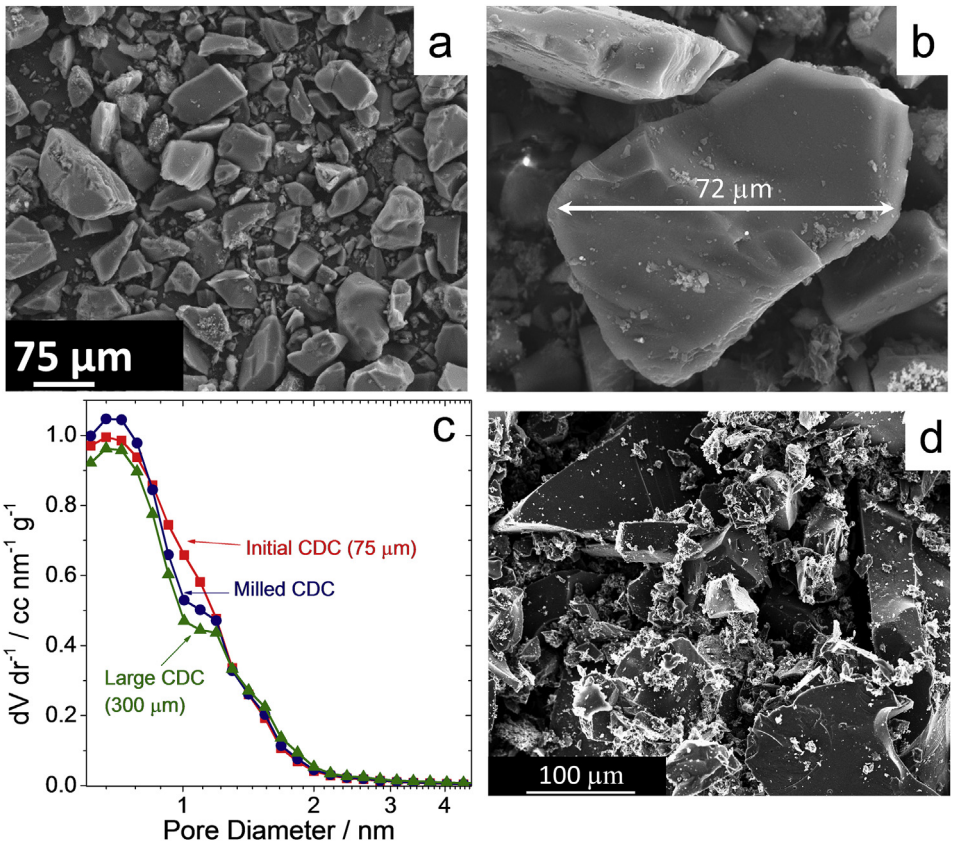

Fig. 1. a) SEM image of coarse-grained CDC powders derived from TiC. b) Higher-magnitude SEM image of a single CDC powder particle. c) Gas sorption-derived pore size distributions of the initial 75 µm diameter coarse-grained CDC, its porosity after mechanical milling, and the pore structure of larger 250 µm diameter CDCs. c) SEM image of larger, 250 µm diameter CDC particles. d) Gas sorption-derived pore size distributions of the initial 75 µm diameter coarse grained CDC, after mechanical milling, and the larger CDC particles.

Table 1
N_2 sorption-derived porosimetry data and TGA-derived ash content of coarse-grained CDC.

Material	BET SSA	DFT SSA	Pore volume	Ash content	Particle diameter
Initial CDC	1822 $m^2\ g^{-1}$	1767 $m^2\ g^{-1}$	0.772 $cm^3\ g^{-1}$	1.91%	75 µm
Milled CDC	1780 $m^2\ g^{-1}$	1729 $m^2\ g^{-1}$	0.755 $cm^3\ g^{-1}$	1.79%	5 µm
Large CDC	1699 $m^2\ g^{-1}$	1433 $m^2\ g^{-1}$	0.759 $cm^3\ g^{-1}$	1.68%	250 µm

within the selected synthesis time and temperatures. The key structural parameters (pore size, carbon ordering, and surface chemistry) of 75–250 µm diameter particles match those of micro- and nano-sized TiC-CDC particles that have been reported in literature.

3.2. Capacitance and rate handling ability

Baseline electrochemical measurements used 2-electrode pouch cell tests of film electrodes (most resembling commercial devices) using 1.5 M $[NEt_4^+][BF_4^-]$ in CH_3CN, which is a typical high-performance electrolyte. Charge/discharge experiments conducted current–voltage sweeps in the 0 – +2.5 V window for YP50 electrodes (4.0 mg cm^{-2} loading) and CDC films (6.2 mg cm^{-2} mass loading) and identical 85 µm film thicknesses. This dimension suggests that coarse-grained CDC films often contain single carbon particles across an entire electrode. From cyclic voltammograms (Fig. 2a) and rate handling analysis, the material demonstrated very high capacitance throughout the entire 2 mV s^{-1} – 1 V s^{-1} sweep range. Cyclic voltammograms demonstrated C_{sp} values as high as 134 F g^{-1} (at 2 mV s^{-1}) and 100 F g^{-1} (at 250 mV s^{-1}). The material retains 44% of its capacitance during 1 V s^{-1} cycling. The cyclic voltammograms maintained a rectangular shape, which suggest minimal electrical or ionic resistance losses during cycling. Furthermore, electrochemical impedance measurements (Fig. 2c) confirmed low equivalent series resistance values (ESR) and minimal contact resistance, as demonstrated by a negligible semicircular Re(Z) vs. −Im(Z) high-frequency region of the Nyquist plot [41,45]. The Bode Impedance plots shown in Fig. 2d demonstrated a near-ideal capacitive behavior at low frequencies (phase (Z) approaches −87° at 10 mHz). The C" (imaginary component of impedance) versus frequency relationship featured a maximum that matched the minimum cell discharge time at a device energy efficiency above 50%. We measured a short 2.95 s time constant, which evidenced the high power capability of the electrode material [46].

The material consistently demonstrated significantly higher charge storage density capabilities than fine-grained activated carbon (YP50) electrode tested under identical conditions. Capacitance of coarse-grained CDC was 31% higher than YP50, and the 75 µm diameter particles demonstrated superior rate handling ability. EIS results for CDC electrodes showed predominantly

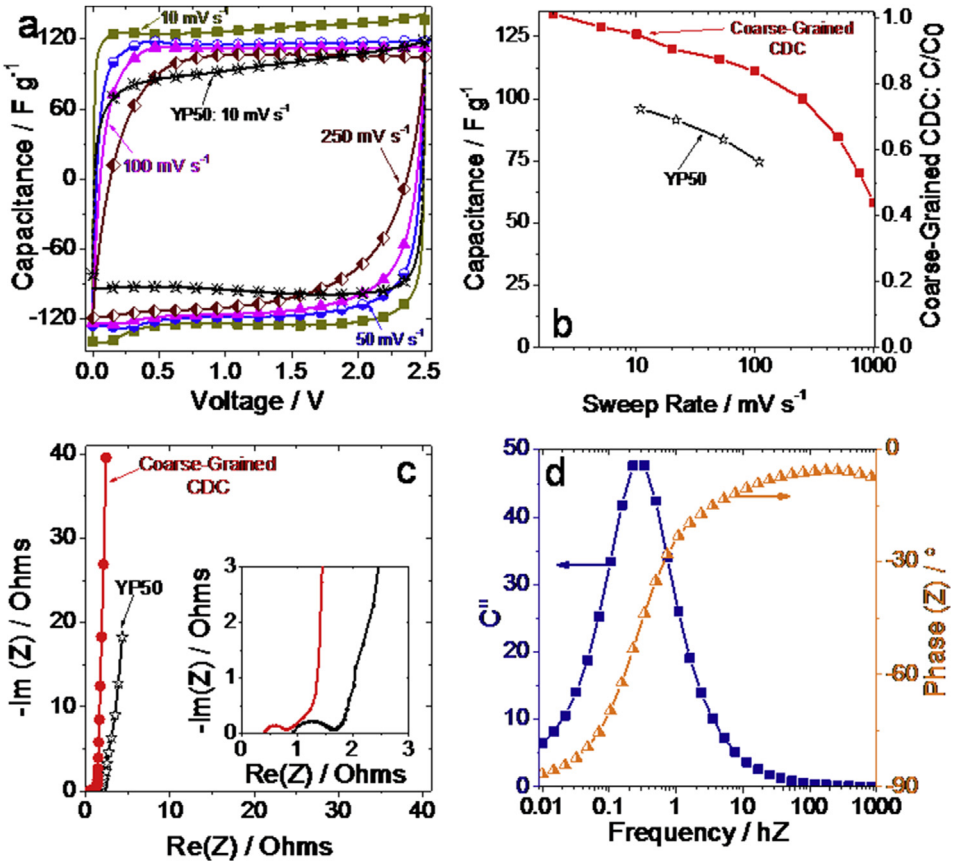

Fig. 2. a) Cyclic voltammograms showing charge/discharge behavior of coarse-grained CDC at 10, 50, 100, and 200 mV s^{-1} in 1.5 M [NEt_4^+][BF_4^-] in acetonitrile, and YP50 activated carbon cycled at 10 mV s^{-1} using the same test cell configuration. b) Comparison of rate handling ability and capacitance retention of CDC and comparison with activated carbon. c) Nyquist plots comparing electronic and ionic resistance of coarse-grained CDC and activated carbon derived from electrochemical impedance spectroscopy. The insert compares the high-frequency regions. d) Phase angle and Bode plots for CDC derived from EIS.

capacitive-dominated impedance at low frequencies (−86.5° for CDC vs. −76.7° for YP50). These materials are compared in Table 2.

An important advantage of coarse-grained CDC particles is the resulting high mass loading of films produced from these materials. The resulting electrodes offer high volumetric energy densities and areal capacitances. Although YP50 can be compacted into electrodes with a 4.0 mg cm^{-2} loading, we produced CDC films with a 6.2 mg cm^{-2} areal density and identical thickness. The cyclic voltammograms, re-normalized by volumetric densities (shown in Fig. S5 in SI), further underscore the advantage of coarse-grained carbons over its activated carbon counterpart.

The same electrode fabrication process successfully increased film thickness from 85 μm to 250–1000 μm to maximize their mass loading. These electrodes retained the same bulk densities and linearly maximized their areal densities to 21.9 mg cm^{-2} (for 250 μm thick films) and 81.2 mg cm^{-2} (for 1 mm thick films). As shown in Fig. 3, the areal capacitance of thicker films improved by 1.8–5.5 times. Although the thicker electrodes exhibited some ion transport limitations (exhibited by increases in impedance and slightly lower capacitance retention) [46], the material still maintained high capacitance and near-rectangular cyclic voltammograms. Randles-Sevcik coefficient calculations showed values above 0.9 for all films (indicating near-ideal capacitive behavior with a minimal diffusion limitation) that did not decrease for thicker films [47]. Impedance comparisons (Fig. 3d) show greater contact resistance (high-frequency region) and lower capacitance (low-frequency region) of 250–1000 μm thick films compared to the 90 μm thick ones and demonstrate that electrode formulations significantly influenced the observed differences in performance. Thicker electrodes likely require different binder ratios, processing/rolling techniques, and other electrode design that is accessible in an industrial setting. These parameters are summarized in Table 3. Subsequently, these coarse-grained CDCs offer a promising approach that maximizes gravimetric and volumetric energy densities without sacrificing rate handling ability or cycling efficiencies at high sweep rates.

Table 2
Comparison of electrochemical performance of CDC and YP50 activated carbon.

Material	C_{sp}, 10 mV s^{-1}	C_{sp}, 100 mV s^{-1}	Time constant	ESR
Initial CDC	129 F g^{-1}	111 F g^{-1}	2.9 s	0.39 Ω
YP50 (Ref.)	96 F g^{-1}	75 F g^{-1}	9.3 s	0.91 Ω

3.3. *Performance in ionic liquid electrolyte*

In addition to evaluating the performance of coarse-grained CDCs in [NEt_4^+][BF_4^-], we also tested the material's capacitance and rate handling abilities in [$EMIm^+$][$TFSI^-$] room-temperature ionic liquid (RTIL) electrolyte. It was examined in both neat (solvent-free) and solvated (50 wt.% concentration in CH_3CN) states; comparison is shown in Fig. 4. These electrodes featured same film thickness and mass loading as shown above. Coarse grained CDC yielded greater capacitance in solvated RTIL than in solvated [NEt_4^+][BF_4^-]: they exhibited a C_{sp} of 148 F g^{-1} (at 10 mV s^{-1}) and maintained high rate handling capability throughout the entire

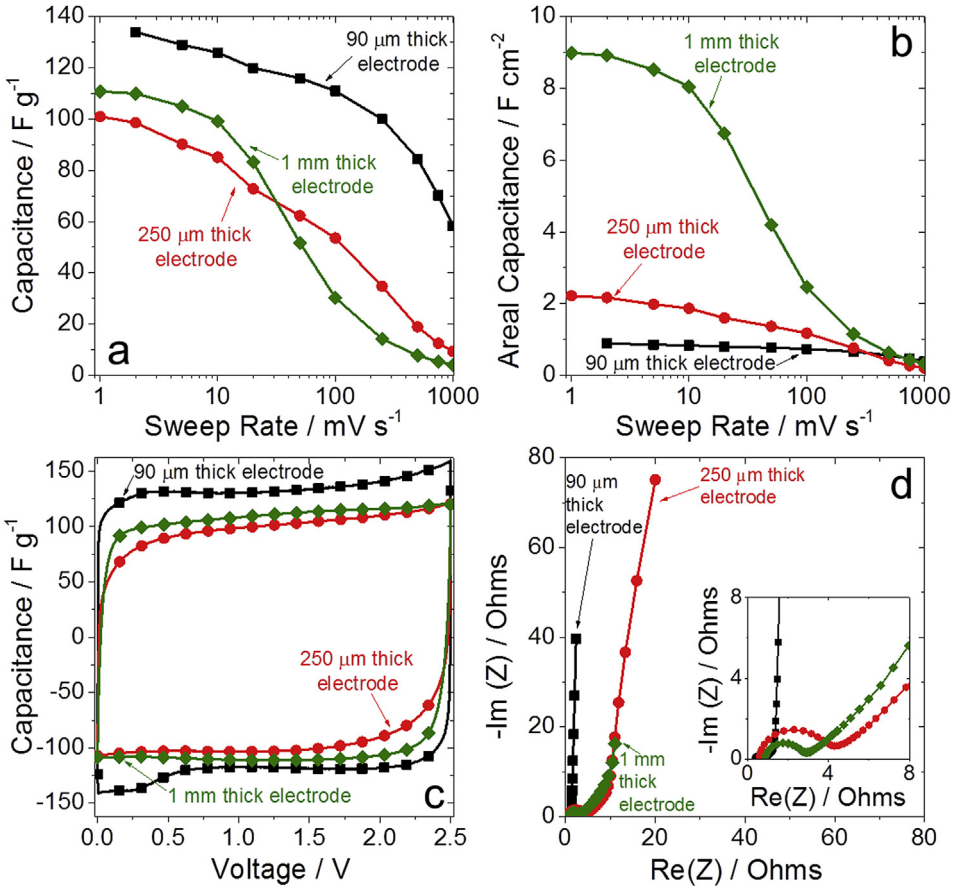

Fig. 3. Rate handling comparison of 90 μm, 250 μm, and 1 mm thick coarse-grained CDC electrode films normalized by a) electrode mass and b) mass loading per unit area. c) Cyclic voltammograms comparing 10 mV s^{-1} cycling of films with different thicknesses in 1.5 M [NEt_4^+][BF_4^-]/acetonitrile electrolyte and d) EIS-derived Nyquist plots for these films.

Table 3
Comparison of key electrochemical metrics, ionic resistance, and diffusion limitations of coarse-grained films with different thicknesses.

Film thickness	C_{sp}, 50 mV s^{-1}	C_{areal}, mV s^{-1}	R_{Ionic}	Randles-Sevcik coefficient
90 μm	116 F g^{-1}	0.77 F cm^{-2}	0.58 Ω	0.947
250 μm	62 F g^{-1}	1.37 F cm^{-2}	5.73 Ω	0.898
1 mm	52 F g^{-1}	4.20 F cm^{-2}	6.67 Ω	0.906

sweep range. The pores of these carbons are sufficiently large to accommodate rapid electrosorption and ion exchange of the larger [$TFSI^-$] and [$EMIm^+$] without ion sieving or transport resistance [14,48]. This optimal electrode-electrolyte pairing further maximized the energy and power density capabilities of coarse-grained CDCs.

We compared the performance of coarse-grained CDCs and YP50 in neat [$EMIm^+$][$TFSI^-$] (same mass loading and film thickness as results shown above) and included those results in Fig. 4. Although capacitance and rate handling abilities of CDC were slightly lower compared to solvated electrolytes (110 F g^{-1} at 10 mV s^{-1}, 25% capacitance retention at 250 mV s^{-1}), they were significantly higher than the measured performance of YP50 electrodes with the same electrolyte. Despite exhibiting smaller particles (shorter pore channels), activated carbon offered 43% lower capacitance (63 F g^{-1} at 10 mV s^{-1}) and matched the rate handling ability of coarse-grained CDC. Therefore, large-diameter porous carbons offer significant performance advantages in applications that require RTIL electrolytes having low conductivity, such as energy storage systems that must operate in broad temperature ranges. The impedance results (shown in Fig. 3d) underscore similar trends: although ionic resistance slightly increases in the mid-frequency region (due to some transport limitations of ions through thicker electrodes), the low-frequency regions are nearly identical and suggest high volumetric power densities of thicker films.

3.4. *Influence of particle size*

We analyzed the influence of particle size by comparing the performance of initial CDC and milled CDC (with the latter featuring 5–20 μm diameter particles) in three different electrolytes. Although the resulting electrodes featured the same 85 μm thickness and similar mass loading (initial CDC: 6.2 mg cm^{-2}, milled CDC: 6.1 mg cm^{-2}), the coarse-grained films exhibited lower resistivity (9.77 Ω cm) compared to those composed of smaller, milled particles (13.60 Ω cm), as shown in Fig. 5. This can be explained by a smaller number of interparticle contacts in the films' cross-section. The performance of CDC electrodes in 1.5 M [NEt_4^+][BF_4^-]/CH_3CN was unaffected by diameter of powders in the electrodes. Both materials exhibited very high capacitance and rate handling ability. When the materials were tested in a more viscous, solvent-free [$EMIm^+$][$TFSI^-$] electrolyte, electrodes with a smaller CDC particle diameter performed better at higher charge/discharge

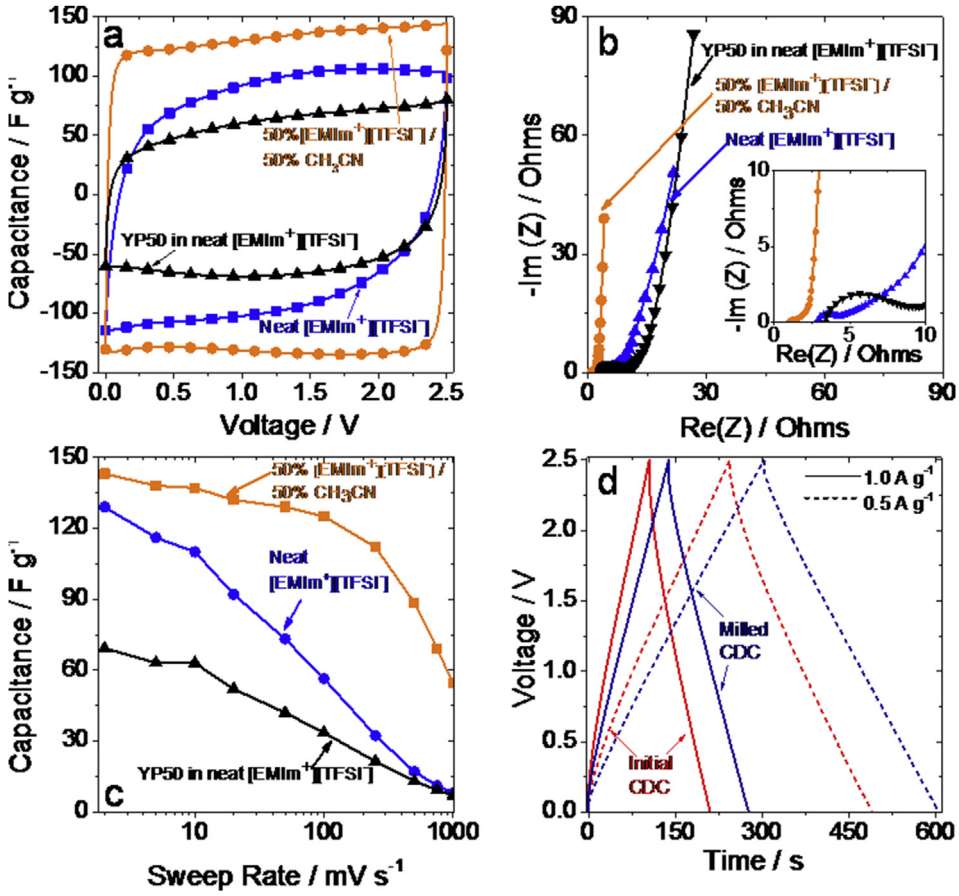

Fig. 4. a) Cyclic voltammograms measured using a 10 mV s^{-1} sweep rate comparing performance of coarse grained CDCs in neat [$EMIm^+$][$TFSI^-$], solvated (50 wt.% solution in acetonitrile) [$EMIm^+$][$TFSI^-$], and YP50 carbon in neat [$EMIm^+$][$TFSI^-$] electrolyte. b) Corresponding EISderived Nyquist plots and c) Rate handling comparisons. d) Charge-discharge galvanostatic cycles recorded at 0.5 A g^{-1} and 1.0 A g^{-1} for initial and milled CDC in neat [$EMIm^+$][$TFSI^-$] electrolyte.

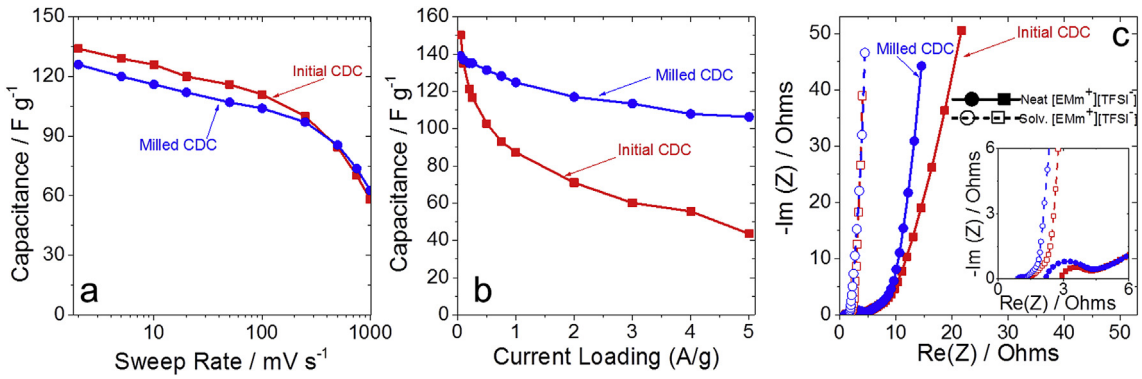

Fig. 5. a) Rate handling and capacitance retention comparison of initial coarse-grained CDCs and an electrode composed of those particles after milling and particle diameter reduction. Tests were conducted in 1.5 M [NEt_4^+][BF_4^-]/acetonitrile electrolyte. b) Current loading comparison (from galvanostatic cycling) for initial and milled CDCs in neat (solvent-free) [EMIm+][TFSI-] ionic liquid electrolyte. c) Nyquist plot comparison of initial and milled CDCs in neat and solvated (50 wt.% solution in acetonitrile) [$EMIm^+$][$TFSI^-$] electrolytes.

rates (56 F g^{-1} for initial CDC vs. 79 F g^{-1} for milled CDC at 100 mV s^{-1}). The materials performed equally well and demonstrated high capacitance regardless of particle size in solvated [$EMIm^+$][$TFSI^-$] in acetonitrile. The Nyquist plots (Fig. 5c) show that ionic resistance of the electrolyte (inside of carbon pores), which is slightly higher for coarse-grained particles in neat RTIL, is equally low for both CDC materials in solvated [$EMIm^+$][$TFSI^-$].

These results present an emerging fundamentally different view of electrosorption. Previous experiments [24] have confirmed the fact that ion motion during electrosorption and dynamic potentials involves localized rearrangement of ions and is not limited by long-range transport of ions across bulk electrolyte [49,50]. Therefore, particles with large diameters (and, subsequently, long pore channels), are capable of demonstrating high capacitance and ion dynamics. In addition to a good electronic conductivity, coarse-grained CDC films offer higher specific surface areas, greater mass

loading, and improved electrolyte accessibility. Although the fundamental explanation for higher capacitance of coarse-grained CDCs will be further explored in the future, larger carbon structures with high conductivity may provide better electrostatic screening of ions and counterions in narrow pores, allow greater charge packing density in pores, and, subsequently, maximize capacitance.

3.5. Electrochemical stability analysis

We examined the electrochemical stability and operating voltage window of CDC electrodes. Galvanostatic cycling was used to charge/discharge them from 0–2.5 V window at 3.0 A g^{-1} for 10,000 cycles in neat [$EMIm^+$][$TFSI^-$] electrolyte. Cycling voltammetry (at 10 mV s^{-1}) quantified capacitance of the material before and after cycling. Furthermore, 2 mV s^{-1} CV sweeps in increasing 0 ↔ 2.5 V–0 ↔ 3.1 V voltage windows (0.1 V increments) evaluated coulombic efficiency and irreversible reactions. Square wave amperommetry measurements identified residual, parasitic currents using 1 h steps from 0.0 V to specific vertex potentials.

Cyclic voltammograms, coulombic efficiencies, and parasitic current analyses are shown in Fig. 6. The material maintains good electrochemical stability up to 3.1 V and minimal potential-induced breakdown throughout the entire tested voltage range. The leakage current of the coarse-grained CDC device at 3.3 V is lower than the specification listed for a commercial supercapacitor (rated to 2.7 V and 350 F) [51]. Cyclic voltammograms did not show a distinct inflection point at high potentials during charge profiles and, subsequently, allowed reversible ion electrosorption in an extended voltage window. After 10,000 cycles in a 0 – +2.5 V voltage window, the material retained most of its capacitance after cycling and only lost 6.7% of its charge storage ability (Fig. S6 in SI). Furthermore, cyclic voltammograms maintained a rectangular shape and did not develop any new redox peaks.

These results show a novel approach for improving the operating voltage windows of porous electrodes. Most previously reported symmetrical CDC electrodes exhibited a 2.5–2.7 V window in bulk organic electrolytes and ionic liquids [52], similar to activated carbons. Coarse-grained CDCs have a large internal surface, with the ratio of ions confined in pores vs. those electrosorbed on the outside of particles significantly greater than for micro- and nano-sized CDCs [17], carbon onions [53], carbon nanotubes [54], and graphene [55]. Since the fundamental properties, densities, and ion-surface interactions of electrolytes fundamentally transform when upon confinement in narrow pores, rates and prevalence of redox reactions and irreversible breakdown (such as ion-surface reactions or catalyzed dimerization [56]) that are driven by an applied potential may drastically change. This is further corroborated by the fact that capacitance degrades by 16.8% for milled CDC electrodes after 10,000 cycles (Table S2 in SI).

3.6. Performance of larger coarse-grained CDCs

In addition to coarse-grained 75 μm TiC-CDC particles, we evaluated the electrochemical performance of 250 μm diameter TiC-CDCs. The thinnest electrodes, which were 280–300 μm thick, also likely used singular particles across entire film. Their performance in 1.5 M [NEt_4^+][BF_4^-]/acetonitrile electrolyte is shown in Fig. 7. Cyclic voltammograms, rate handling analyses, and Nyquist plots also include results from 280 μm thick films composed of 75 μm diameter particles – the closest electrode comparison. The large, 250 μm particle CDC films included a 5 wt. % carbon nanotube additive to maximize conductivity and replicate the most typical composition of commercial supercapacitor electrode.

The larger particles demonstrate equally high capacitance and are capable of delivering over 110 F g^{-1} at 10 mV s^{-1}. As with all prior experiments, the cyclic voltammograms maintained a rectangular shape and did not demonstrate any ion sieving (Fig. 6a). This finding establishes a clear trend for coarse-grained particles with long pore lengths: they showcase high capacitance and electrosorption rate abilities. The ~280 μm films composed of these larger particles offered greater rate handling capabilities than identically thick electrodes composed of smaller particles (Fig. 6b). Across the 2–200 mV s^{-1} sweep range, C_{sp} for large CDCs was 20–30 F g^{-1} larger than that for 75 μm ones. Nyquist plots (Fig. 6c) showed lower ionic resistance in larger particles, especially at low oscillating frequencies. The ESRs of 250–300 μm thick films were approximately the same (0.71 Ω for 250 μm CDC particles, 0.57 Ω for 75 μm particles). Contact impedance (the semi-circular high-frequency region) was significantly lower for the larger-particle CDC, and both improved electron transport through the large-particle films and the conductive additive likely contributed to the favorable electrode-current collector interface. Furthermore, the ionic impedance was significantly lower in the 250 μm diameter particle films: 1.71 Ω, versus 5.73 Ω for 75 μm CDCs. These differences demonstrate advantage of electrode films with fewer particles across film thickness, as reduced void space between particles minimizes bulk ion transport and improves capacitance and ion dynamics.

Although 75 μm diameter CDCs are more cost-effective than micropowder and nanopowder CDCs, 250 μm diameter CDCs are less expensive than all other alternatives. They require no ball-milling and expand the catalog of precursor carbide materials and suppliers. These films exhibit high mass loading densities – 15.2 mg cm^{-2} – and are suitable in a broad range of grid storage and automotive applications. Most importantly, these results

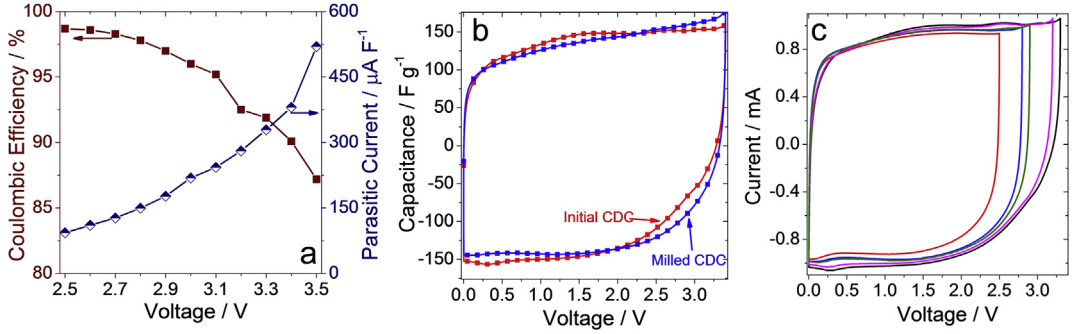

Fig. 6. a) Comparison of coulombic efficiency (from cyclic voltammetry at 2 mV s^{-1}) and steadystate current measurements (from 60-min square wave amperommetry) in the 2.5–3.5 V electrochemical window for initial (75 μm diameter) CDCs. b) Cyclic voltammograms comparing initial CDC and milled CDC cycled in neat [$EMIm^+$][$TFSI^-$] electrolyte at 2 mV s^{-1} in the 0.0–3.4 V window. c) First-cycle CVs of initial CDC electrodes cycled between a 0–2.5 V and a 0–3.5 V window with a 0.1 V increment between each sweep.

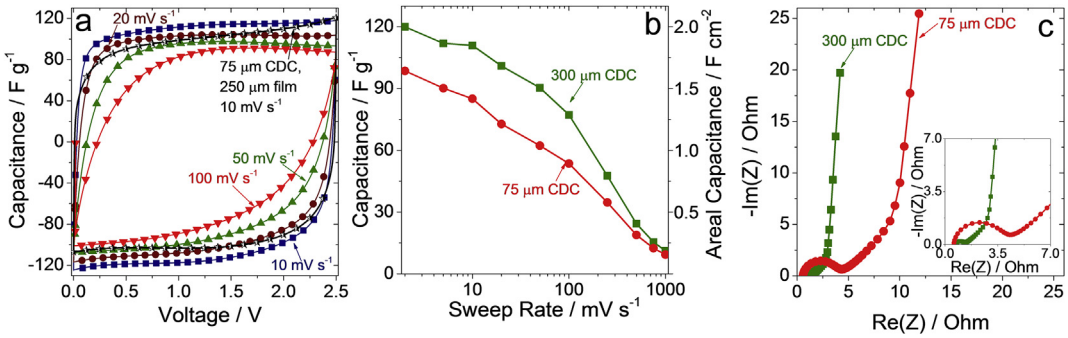

Fig. 7. a) Cyclic voltammograms of TiC-CDC films composed of 250 μm diameter particles at 10 mV s^{-1}, 20 mV s^{-1}, 50 mV s^{-1}, and 100 mV s^{-1}. Data is shown for 1.5 M [NEt_4^+][BF_4^-]/acetonitrile. b) Rate handling ability and c) Nyquist impedance plot of larger CDC electrodes in organic electrolyte. For comparison, performance for a similarly thick (250 μm) electrode composed of 75 μm diameter TiC-CDCs is included in a), b), and c). The time constant for the 250 μm CDC film was 12.6 s, versus 10.4 s for a similarly thick film composed of 75 μm particles.

demonstrated a clear trend that large porous particles are capable of high capacitance and are not impeded by near-infinite pore lengths. Some limitations, however, become more apparent at higher sweep rates; the material's optimal cycling performance lies in the 1–200 mV s^{-1} charge/discharge range. The significance of ion transport through long pore lengths becomes more prevalent at high loads and in more viscous electrolytes. Although 250 μm CDCs performed adequately well in neat [$EMIm^+$][$TFSI^-$] at 10 mV s^{-1} (62 F g^{-1}), their performance rapidly decayed at higher sweep rate. These results are shown in Fig. S7 in SI.

4. Summary

We demonstrated high capacitance and rate handling ability of coarse-grained carbide derived carbons in different electrolytes. These electrode materials are easier and less expensive to produce, and offer high areal densities. The resulting electrodes from these carbons can reach 1 mm thickness and still offer high charge storage and charge/discharge rates. As of present date, no electrodes with such thickness and adequate performance have been reported in literature. The resulting increases in areal capacitance and volumetric energy densities make these 75 μm diameter particles viable electrical energy storage materials for a broad range of automotive and grid storage applications. These materials demonstrate a high electrochemical stability and can operate in a 3.1 V voltage window, which further maximizes their energy density. This effect extends to larger carbon particles; 250 μm diameter particles that require even smaller processing costs, exhibit equally high capacitance in organic electrolytes.

Our findings challenge the conventional assumption that long, tortuous pore channels in coarse-grained carbons substantially impede ion transport and are unsuitable for high-performance energy storage systems. We provide additional evidence of the concept that electrosorption is a short-ranged, localized process. Although our results provide some fundamental insights into the charge storage mechanism, this issue must be explored further with additional materials characterization, electrochemical testing, and novel computational analysis and modeling work. Furthermore, although we relied on a standard electrode preparation technique, further optimization of film preparation and structure is needed to fully capitalize on the capabilities of this material. Electrodes will offer even greater energy and power densities if they include conductive additives (carbon black and onion-like carbons), optimized film structure for greater ion accessibility, and improved film rolling techniques on an industrial production scale.

Acknowledgments

This study was supported by the Fluid Interface Reactions, Structures and Transport (FIRST) Center, an Energy Frontier Research Center funded by the U.S. Department of Energy, Office of Science, Office of Basic Energy Sciences. X-ray scattering measurements (at ANL) and EQ-SANS measurements (at ORNL) were made available through the Scientific User Facilities Division, Office of Basic Energy Sciences, US Department of Energy. The authors thank Hsiu-Wen Wang and Katharine Page (Oak Ridge National Laboratory) for their assistance with X-Ray PDF measurements and data reduction. William Heller and Gernot Rother (Oak Ridge National Laboratory) assisted with EQ-SANS data collection and reduction. The authors thank Eu Ju Moon (Drexel University) for assistance with conductivity measurements and Sankalp Kota and Babak Anasori (Drexel University) for assistance with SEM and EDS.

Appendix A. Supplementary data

Supplementary data related to this article can be found at http://dx.doi.org/10.1016/j.jpowsour.2015.11.099.

References

[1] P. Simon, Y. Gogotsi, Accounts of Chemical Research, 46, 2013, pp. 1094–1103.
[2] P. Simon, Y. Gogotsi, Nat. Mater. 7 (2008) 845–854.
[3] P. Simon, Y. Gogotsi, B. Dunn, Science 343 (2014) 1210–1211.
[4] F. Béguin, V. Presser, A. Balducci, E. Frackowiak, Adv. Mater. 26 (14) (2014) 2219–2251.
[5] M. Beidaghi, Y. Gogotsi, Energy Environ. Sci. 7 (2014) 867–884.
[6] K. Jost, G. Dion, Y. Gogotsi, J. Mater. Chem. A 2 (2014) 10776–10787.
[7] A.G. Pandolfo, A.F. Hollenkamp, J. Power Sources 157 (2006) 11–27.
[8] C. Schütter, C. Ramirez-Castro, M. Oljaca, S. Passerini, M. Winter, A. Balducci, J. Electrochem. Soc. 162 (2015) A44–A51.
[9] T. Ariyanto, B. Dyatkin, G.-R. Zhang, A. Kern, Y. Gogotsi, B.J.M. Etzold, Microporous Mesoporous Mater. 218 (2015) 130–136.
[10] V. Presser, M. Heon, Y. Gogotsi, Adv. Funct. Mater. 21 (2011) 810–833.
[11] Y. Gogotsi, V. Presser, Carbon Nanomaterials, second ed., CRC Press, 2013.
[12] C. Largeot, C. Portet, J. Chmiola, P.-L. Taberna, Y. Gogotsi, P. Simon, J. Am. Chem. Soc. 130 (2008) 2730–2731.
[13] J. Chmiola, G. Yushin, Y. Gogotsi, C. Portet, P. Simon, P.L. Taberna, Science 313 (2006) 1760–1763.
[14] L. Allen, Z. Ranyi, M. McNallan, J. Phys. Condens. Matter 18 (2006) S1763.
[15] R. Lin, P. Huang, J. Ségalini, C. Largeot, P.L. Taberna, J. Chmiola, Y. Gogotsi, P. Simon, Electrochim. Acta 54 (2009) 7025–7032.
[16] Y. Gogotsi, A. Nikitin, H. Ye, W. Zhou, J.E. Fischer, B. Yi, H.C. Foley, M.W. Barsoum, Nat. Mater. 2 (2003) 591–594.
[17] C.R. Perez, S.-H. Yeon, J. Segalini, V. Presser, P.-L. Taberna, P. Simon, Y. Gogotsi, Adv. Funct. Mater. 23 (2013) 1081–1089.
[18] L. Tong, R.G. Reddy, Scr. Mater. 52 (2005) 1253–1258.
[19] C. Portet, G. Yushin, Y. Gogotsi, J. Electrochem. Soc. 155 (2008) A531–A536.
[20] K. Xia, Q. Gao, J. Jiang, J. Hu, Carbon 46 (2008) 1718–1726.
[21] H. Nishihara, H. Itoi, T. Kogure, P.-X. Hou, H. Touhara, F. Okino, T. Kyotani, Chem. A Eur. J. 15 (2009) 5355–5363.

[22] D.-W. Wang, F. Li, M. Liu, G.Q. Lu, H.-M. Cheng, Angew. Chem. Int. Ed. 47 (2008) 373–376.
[23] Y. Mun, C. Jo, T. Hyeon, J. Lee, K.-S. Ha, K.-W. Jun, S.-H. Lee, S.-W. Hong, H.I. Lee, S. Yoon, J. Lee, Carbon 64 (2013) 391–402.
[24] F.W. Richey, B. Dyatkin, Y. Gogotsi, Y.A. Elabd, J. Am. Chem. Soc. 135 (2013) 12818–12826.
[25] V. Presser, C.R. Dennison, J. Campos, K.W. Knehr, E.C. Kumbur, Y. Gogotsi, Adv. Energy Mater. 2 (2012) 895–902.
[26] C.R. Dennison, M. Beidaghi, K.B. Hatzell, J.W. Campos, Y. Gogotsi, E.C. Kumbur, J. Power Sources 247 (2014) 489–496.
[27] J. Chmiola, C. Largeot, P.-L. Taberna, P. Simon, Y. Gogotsi, Science 328 (2010) 480–483.
[28] M. Heon, S. Lofland, J. Applegate, R. Nolte, E. Cortes, J. Hettinger, P. Taberna, P. Simon, P. Huang, M. Brunet, Y. Gogotsi, Energy Environ. Sci. 4 (2011) 135–138.
[29] S.-H. Yeon, I. Knoke, Y. Gogotsi, J.E. Fischer, Microporous Mesoporous Mater. 131 (2010) 423–428.
[30] M.-C. Liu, L.-B. Kong, P. Zhang, Y.-C. Luo, L. Kang, Electrochim. Acta 60 (2012) 443–448.
[31] J. Huang, B.G. Sumpter, V. Meunier, G. Yushin, C. Portet, Y. Gogotsi, J. Mater. Res. Soc. 25 (2010) 1525–1531.
[32] J. Huang, B.G. Sumpter, V. Meunier, Chem. A Eur. J. 14 (2008) 6614–6626.
[33] R. Dash, J. Chmiola, G. Yushin, Y. Gogotsi, G. Laudisio, J. Singer, J. Fischer, S. Kucheyev, Carbon 44 (2006) 2489–2497.
[34] R.K. Dash, G. Yushin, Y. Gogotsi, Microporous Mesoporous Mater. 86 (2005) 50–57.
[35] S. Brunauer, P.H. Emmett, E. Teller, J. Am. Chem. Soc. 60 (1938) 309–319.
[36] G.Y. Gor, M. Thommes, K.A. Cychosz, A.V. Neimark, Carbon 50 (2012) 1583–1590.
[37] V.N. Mochalin, I. Neitzel, B.J.M. Etzold, A. Peterson, G. Palmese, Y. Gogotsi, ACS Nano 5 (2011) 7494–7502.
[38] J.L. Bañuelos, G. Feng, P.F. Fulvio, S. Li, G. Rother, S. Dai, P.T. Cummings, D.J. Wesolowski, Chem. Mater. 26 (2014) 1144–1153.
[39] M.D. Stoller, R.S. Ruoff, Energy Environ. Sci. 3 (2010) 1294–1301.
[40] J. Halim, M.R. Lukatskaya, K.M. Cook, J. Lu, C.R. Smith, L.-Å. Näslund, S.J. May, L. Hultman, Y. Gogotsi, P. Eklund, M.W. Barsoum, Chem. Mater. 26 (2014) 2374–2381.
[41] C. Portet, P.L. Taberna, P. Simon, C. Laberty-Robert, Electrochim. Acta 49 (2004) 905–912.
[42] K. Faber, F. Badaczewski, M. Oschatz, G. Mondin, W. Nickel, S. Kaskel, B.M. Smarsly, J. Phys. Chem. C 118 (2014) 15705–15715.
[43] G. Laudisio, R.K. Dash, J.P. Singer, G. Yushin, Y. Gogotsi, J.E. Fischer, Langmuir 22 (2006) 8945–8950.
[44] M.A. Smith, H.C. Foley, R.F. Lobo, Carbon 42 (2004) 2041–2048.
[45] P.L. Taberna, P. Simon, J.F. Fauvarque, J. Electrochem. Soc. 150 (2003) A292–A300.
[46] J. Segalini, B. Daffos, P.L. Taberna, Y. Gogotsi, P. Simon, Electrochim. Acta 55 (2010) 7489–7494.
[47] J. Lim, P. Malati, F. Bonet, B. Dunn, J. Electrochem. Soc. 154 (2007) A140–A145.
[48] N.N. Rajput, J. Monk, R. Singh, F.R. Hung, J. Phys. Chem. C 116 (2012) 5169–5181.
[49] W.-Y. Tsai, P.-L. Taberna, P. Simon, J. Am. Chem. Soc. 136 (2014) 8722–8728.
[50] J.M. Griffin, A.C. Forse, W.-Y. Tsai, P.-L. Taberna, P. Simon, C.P. Grey, Nat. Mater. 14 (2015) 812–819.
[51] in, Maxwell, 2013, pp. 1–5.
[52] K.L. Van Aken, M. Beidaghi, Y. Gogotsi, Angew. Chem. Int. Ed. 54 (2015) 4806–4809.
[53] K.L. Van Aken, J.K. McDonough, S. Li, G. Feng, S.M. Chathoth, E. Mamontov, P.F. Fulvio, P.T. Cummings, S. Dai, Y. Gogotsi, J. Phys. Condens. Matter 26 (2014) 284104.
[54] C. Portet, G. Yushin, Y. Gogotsi, Carbon 45 (2007) 2511–2518.
[55] H. Ji, X. Zhao, Z. Qiao, J. Jung, Y. Zhu, Y. Lu, L.L. Zhang, A.H. MacDonald, R.S. Ruoff, Nat. Commun. 5 (2014) 3317.
[56] T. Romann, O. Oll, P. Pikma, H. Tamme, E. Lust, Electrochim. Acta 125 (2014) 183–190.